NASA/TM—2001-210679

Computational Analysis of the Combustion Processes in an Axisymmetric, RBCC Flowpath

Christopher J. Steffen, Jr.
Glenn Research Center, Cleveland, Ohio

Shaye Yungster
Institute for Computational Mechanics in Propulsion, Cleveland, Ohio

Prepared for the
37th Combustion Subcommittee, 25th Airbreathing Propulsion Subcommittee, and
19th Propulsion Systems Hazards Subcommittee Joint Meeting
cosponsored by the Joint Army-Navy-Air Force Interagency Propulsion Committee
Monterey, California, November 13–17, 2000

National Aeronautics and
Space Administration

Glenn Research Center

February 2001

This report is a formal draft or working paper, intended to solicit comments and ideas from a technical peer group.

This report contains preliminary findings, subject to revision as analysis proceeds.

Available from

NASA Center for Aerospace Information
7121 Standard Drive
Hanover, MD 21076
Price Code: A03

National Technical Information Service
5285 Port Royal Road
Springfield, VA 22100
Price Code: A03

Available electronically at http://gltrs.grc.nasa.gov/GLTRS

COMPUTATIONAL ANALYSIS OF THE COMBUSTION PROCESSES IN AN AXISYMMETRIC, RBCC FLOWPATH

Christopher J. Steffen, Jr.*
National Aeronautics and Space Administration
Glenn Research Center
Cleveland, Ohio 44135

Shaye Yungster◇
Institute for Computational Mechanics in Propulsion
Brook Park, Ohio 44135

ABSTRACT

Computational fluid dynamic simulations have been used to study the combustion processes within an axisymmetric, RBCC flowpath. Two distinct operating modes have been analyzed to date, including the independent ramjet stream (IRS) cycle and the supersonic combustion ramjet (scramjet) cycle. The IRS cycle investigation examined the influence of fuel-air ratio, fuel distribution, and rocket chamber pressure upon the combustion physics and thermal choke characteristics. Results indicate that adjustment of the amount and radial distribution of fuel can control the thermal choke point. The secondary massflow rate was very sensitive to the fuel-air ratio and the rocket chamber pressure. The scramjet investigation examined the influence of fuel-air ratio and fuel injection schedule upon combustion performance estimates. An analysis of the mesh-dependence of these calculations was presented. Jet penetration data was extracted from the three-dimensional simulations and compared favorably with experimental correlations of similar flows. Results indicate that combustion efficiency was very sensitive to the fuel schedule.

INTRODUCTION

BACKGROUND

NASA is presently studying several advanced propulsion systems that promise to provide affordable access to space. The John H. Glenn Research Center is focusing on the development and demonstration of several low-risk approaches to Air-Breathing Launch Vehicle technologies. One concept, the reusable SSTO "GTX", is based upon Rocket Based Combined Cycle (RBCC) propulsion. A three-view schematic is shown in Figure 1. Vehicle propulsion is the critical technology for GTX. However, design simplicity is the key attribute. Therefore, a nearly axisymmetric engine design has been created. Structural and analytical simplicity results.

The RBCC concept considered here is defined by four separate modes in a single-stage-to-orbit configuration. First, the engine functions with the rocket ignited in a unique Ejector-Ramjet cycle[1] (mode 1). Then the rocket engine is switched off and subsonic combustion is present in the ramjet (mode 2). As the vehicle continues to accelerate, supersonic combustion occurs in the Scramjet (mode 3). The rocket is eventually re-ignited (mode 4) for the final ascent into orbit in an all-rocket configuration. Further details on the operation of this propulsion cycle are available in reference[2].

A single flowpath is used throughout the four propulsion modes. This geometric simplicity presents a complex design challenge for the air-breathing combustor. Location of the fuel injection ports must optimize the performance of the entire air-breathing portion of the trajectory. CFD offers an efficient analysis method, when coupled with ongoing experimental efforts, to estimate combustor efficiencies and generate 3D design-specific fluids analysis. The current work discusses the computational combustor

*Engine Systems Technology Branch, c.j.steffen@grc.nasa.gov

◇shaye.yungster@grc.nasa.gov

analysis for Mode 1 and Mode 3. In turn, this analysis guides us toward more accurate 1D combustion modeling for cycle analysis and trajectory optimization.

The present study is presented in two distinct phases, defined by the separate operating modes. The first section of this paper deals with a computational analysis of the low speed (mode #1) combustor. The numerical models and results applicable to mode #1 analysis are presented together in one section. The second section of this paper deals with the analysis and results applicable to the high speed (mode #3) combustor. This second section includes a separate presentation of the numerical models and results. This work represents an overview of the computational combustion analysis that is currently underway within the GTX program.

LOW SPEED COMBUSTOR ANALYSIS

MODE 1: EJECTOR-RAMJET MODE (IRS CYCLE)

The Independent Ramjet Stream (IRS) cycle, a variation of the conventional ejector-ramjet, is currently being evaluated for use as the low speed propulsion mode of GTX. This propulsion mode typically covers the speed range from lift-off to a maximum around Mach 3. In a conventional ejector-ramjet, a fuel-rich rocket exhaust is mixed and burned with air captured by the inlet. The rocket provides all of the fuel needed for combustion with the entrained air. The internal flowpath is designed to produce thermal choking where mixing is complete. The main disadvantage of this concept is the relatively long duct required to achieve complete mixing of the air and rocket streams. In order to overcome this difficulty, a modification of the conventional ejector-ramjet was proposed in which the requirement for complete mixing of the two streams is removed. Removing the requirement for mixing can shorten the flowpath considerably, with a corresponding reduction in structural weight and wetted area. Another benefit is a reduction in risk and complexity since a single rocket element can now be used without regard for mixing length. Also, higher thermodynamic performance is possible in other modes where a shorter mixing duct would reduce expansion process losses.

In the IRS cycle, the airstream is fueled independently using the ramjet and scramjet mode fuel injectors located in the inlet diffuser, as shown in Figure 3. The rocket serves as a pilot for the fueled airstream. This can be accomplished upstream, since the air stagnation temperatures during this mode are not high enough to cause autoignition. When the premixed fuel-air stream makes contact with the rocket plume, it is ignited (see Figure 3) and a flame propagates across the combustor duct forming a thermal throat. The length of the flowpath is now determined by the flame propagation speed. Since the rocket is not the fuel source for the airstream, the rocket oxidizer-to-fuel ratio (O/F) can be fixed at an optimum value for best system performance. An additional advantage of the IRS cycle is that the fuel injectors provide the means to control the location of the thermal throat by adjusting the amount and radial distribution of the fuel injected into the airstream.

The goal of this mode 1 study is to conduct a CFD investigation of the IRS cycle on an axisymmetric engine configuration having the same area distribution as the GTX engine flowpath. The objective is to understand the flow and combustion physics, thermal choke characteristics, and the effects of airstream fuel-air ratio, mixture distribution, and rocket chamber pressure on flame propagation and stability.

NUMERICAL METHOD

The analysis of the IRS cycle is carried out using a specialized CFD code developed in-house for computing reacting flows, and is described in Yungster and Radhakrishnan[3]. It solves the axisymmetric Navier-Stokes equations including finite-rate chemistry and real gas effects using an implicit, total variation diminishing (TVD) algorithm. It includes a generalized detailed chemistry capability, various options for turbulence models, and steady-state or time accurate marching algorithms. In particular, the Spalart-Allmaras[4] one-equation turbulence model was used in this study.

The chemical reaction mechanism for hydrogen-air combustion was based on Jachimowski's model[5], except reactions involving N2, HO2 and H2O2 are not considered. Nitrogen reactions become important only at higher Mach numbers than considered here, and reactions involving HO2 and H2O2 are of secondary importance for this application. The simplified reaction mechanism, consisting of 8 elementary reactions among 6 reacting species and the inert species N2, results in significant savings in CPU time.

The numerical method used for solving the Navier-Stokes and species transport equations is described in detail in reference 3 and briefly summarized below. The equation set is discretized using the backward differentiation formula (BDF) method, because its accuracy and efficiency in solving the differential equations arising in combustion chemistry have been well established[6].

The numerical fluxes are discretized using Yee's second order total variation diminishing (TVD) scheme[7]. The resulting equation is then linearized in a conservative manner and solved iteratively, by using a lower-upper relaxation procedure consisting of successive Gauss-Seidel (LU-SGS) sweeps.

The inversion of large matrices is avoided by partitioning the system into reacting and nonreacting parts. Consequently, the matrices that have to be inverted are of the same size (NxN), where N is the number of reacting species as those that arise in the commonly used point implicit methods. An important advantage of the present method is that, because it is fully implicit, it is stable for large values of the CFL number, thereby enabling the use of relatively large time steps to minimize computational cost. Steady state was achieved when the mass flux was resolved to within 1% across the domain.

RESULTS

In this paper, we present results from several numerical simulations of the IRS cycle that illustrate the effects of one particular parameter (at a given Mach number) on the flow and combustion characteristics of a specific axisymmetric engine configuration, which is shown in Figure 2. The area distribution was selected to correspond to that in the engine flowpath of the GTX vehicle. A plug nozzle rocket configuration is used to provide pressure compensation as the rocket is throttled down and ram pressure increases with Mach number.

The boundary conditions are as follows: For the inflow plane of both the primary (rocket) and secondary (airflow) streams the total pressure and total temperature were specified. Adiabatic walls were assumed, and the exit plane used a mixed subsonic/supersonic boundary condition. When the local Mach number exceeded one, all variables were extrapolated. For regions of subsonic flows, an exit pressure was specified. In all the calculations, the rocket operated at an oxygen-fuel ratio of six.

The IRS propulsion mode covers the speed range from lift-off to a maximum around Mach 3. Results are presented for Mach numbers of 1.0, 1.5 and 2.0. For the M=1 conditions, two different secondary flow models are investigated as discussed below. At the M=1.5 flight condition we studied the effects of secondary flow equivalence ratio (ϕ), and at M =2 we show the effects of rocket chamber pressure on the flowfield.

Figure 4 and Figure 5 show the results for M = 1. Figure 4 shows the results of a computation that assumes the secondary stream consists of a hydrogen-air gas mixture at an equivalence ratio, ϕ=0.6. That is, we are assuming that hydrogen injection occurred further upstream, and a premixed hydrogen-air secondary stream is flowing into the combustor. In order to examine the effects of nonuniform mixing, we carried out a computation in which hydrogen is injected through two axial sonic injectors. The results of this simulation are shown in Figure 5. The equivalence ratio was (ϕ=0.4) for this case.

The results shown in Figure 4 and Figure 5 are presented in the form of O2 mass fraction, nondimensional temperature and pressure, and Mach number contours. The O2 plot clearly shows the flame front propagating across the secondary stream, and, in the case of Figure 5, shows the hydrogen injection as regions of lower O2 concentration. The black colored region indicates the rocket exhaust, which has no excess oxygen. The temperature plot also shows the flame front and the mixing region. This region, located between the rocket exhaust and the flame front, is characterized by a higher temperature due to the combustion of the excess hydrogen in the rocket stream, which has been mixed with secondary air. The pressure plot shows the high pressure produced in the front part of the combustor due to the thermal choking. Also, at these M=1 conditions, there is not sufficient pressure differential across the combustor to drive the secondary flow completely supersonic, and as a result a shock wave forms near the exit of the combustor. The final two plots in Figure 4 and Figure 5 show Mach number contours. The fourth pair of images shows the overall Mach number range, while the fifth and final pair show only the subsonic flow regions.

The thermal choke mechanism can be clearly seen from this (and subsequent) figures. The flame propagating across the secondary stream creates an aerodynamic throat that forces the remaining unburned

secondary flow to choke. As the velocity of the secondary stream increases, the flame angle decreases and in fact the flame never reaches the top wall. Note also that near the exit of the combustor the secondary stream shocks down to subsonic speeds and the flame angle increases slightly but not enough to reach the top wall before the end of the combustor. Note also that the thermal throat location occurs further downstream in Figure 5 as compared to Figure 4. This indicates that by adjusting the amount and radial distribution of fuel it is possible to control the location of the thermal throat and therefore, to control the combustor pressure and secondary airflow.

The remaining cases (for M=1.5 and M=2) have all been computed assuming a premixed hydrogen-air secondary stream. Figure 6 shows results for M=1.5 conditions and for three different values of the secondary flow equivalence ratio, (ϕ=0.6, 0.7, & 0.8). This figure plots contours of the subsonic flow region and temperature contours. Note that by increasing ϕ, the flame penetrates deeper into the secondary stream, and the flame becomes steeper in its initial portion. It subsequently flattens out due to the increased velocity in the secondary stream. The flame does not reach the combustor wall in any of these cases. The airflow is very sensitive to increases in equivalence ratio, since as ϕ is increased and more heat is released, the airflow decreases resulting in lower velocities in the secondary stream. As a result of the lower velocities, the flame can propagate deeper across the combustor and reduce airflow even more. The aerodynamic throat occurs approximately at the same axial location, but the available area of the nonreacting flow decreases with increasing ϕ. As a result the amount of airflow decreases. The parameter β represents the secondary-to-primary total mass flow ratio. The mass flow ratio decreases from β=2.74 for ϕ=0.6 to β=2.00 for ϕ=0.8. Note also that for the conditions at M=1.5, the entire flow is supersonic at the exit plane. (The white areas in the Mach number plots in Figure 6 represent Mach number values higher than one).

Figure 7 shows three cases for the M=2 conditions. These calculations were made with a secondary flow equivalence ratio of (ϕ=0.6), but for three different values of the rocket chamber pressure, Pc. This figure shows that when Pc is reduced from 1393 psi to 1000 psi, the rocket exhaust expansion is lower as expected. As a result, the flame penetration into the secondary flow is also reduced and therefore more air can flow through the engine. As Pc is reduced further to 700 psi, the secondary stream goes supersonic shortly after the constant area section. This short supersonic region is followed by a normal shock. The flow then thermally chokes in a manner similar to the previous cases. Therefore, at Pc=700 psi more fuel is needed in order to push out the normal shock out of the domain.

HIGH SPEED COMBUSTOR ANALYSIS

MODE 3: SCRAMJET

The GTX vehicle is expected to operate in the Scramjet mode from about Mach 6-11. The fuel injectors have been laid-out to maximize combustion efficiency. This is achieved by properly locating the combustion process along the flowpath with an optimal fuel schedule. A combination of axial and normal injectors have been specified as shown in Figure 8. The engine configuration specified for these simulations corresponds to an inlet contraction ratio of 12. At this contraction ratio, the inlet throat is defined by the alignment of two backward-facing steps at the same axial location, one each for the centerbody and cowl surfaces. The axial fuel injectors supply a small amount of hydrogen in the flame holding regions of the backward facing steps. Just downstream of the flameholding region, the second row of injectors has been located and oriented to inject fuel into the stream through transverse ports. Strict normal injection from the centerbody yielded a small, positive axial component. Strict radial injection from the cowl has been specified to avoid the negative axial component of velocity. Thus, all cowl injectors have been slightly inclined into the streamwise direction.

The axial injectors have been placed with a 3-degree pitch between adjacent ports. The second and third rows of injectors have been placed at a 6-degree pitch, while the fourth row has been placed at a 12-degree pitch. The CFD simulation takes advantage of the symmetry conditions as much as possible to minimize the computational effort required. For the first two simulations executed, a 6-degree pitch dictated the symmetry condition of a 3-degree domain. The third simulation required the resolution of the 12-degree pitch, so that a 6-degree domain was specified. This was accomplished by simply doubling the computational mesh in size. Thus a similar mesh density was used for all cases. Note that the use of

symmetry planes implies the simulation of a full 360-degree engine. This differs from the actual GTX reference vehicle geometry, which is comprised of an approximately 215 degree sector with sidewalls.

The goal of this mode #3 study was to perform a series of 3D calculations of the scramjet combustion process that can be (1) analyzed for mesh dependence of the performance results (CFD verification) and (2) compared to the performance results of upcoming free-jet tests (CFD validation). The current simulations have been conducted at a fixed inflow condition. Three different fuel schedules have been examined, at ϕ=0.6,0.8 and 1.0. The calculations at ϕ=0.6 have been repeated with a fine mesh that is doubled in each coordinate direction (eight times as many grid points) to enable an assessment of the mesh dependency of the calculations.

NUMERICAL MODELS

The flow solver GASP v3.2[8] from Aerosoft, Inc. was used to conduct the analysis. The solver was configured to the following specifications:

- Third-order-accurate upwind biased scheme
- Minmod limiting strategy
- Roe's approximate Reimann solver
- Two-factor ADI algorithm
- Low Re_t k-ω turbulence model
- Drummond et al[9] model for air/H2 chemical kinetics (9 species/18 reactions)
- Thermodynamic equilibrium assumed for translational, rotational, and vibrational energy modes, using the LeRC curve fits[10]

The mesh was developed with Gridgen[11] software from Pointwise, Inc. The mesh consisted of 260(axial) x 152(radial) x 32(spanwise) cells over a three-degree annular sector. For the six-degree mesh, the dimensions were (260x152x64). This mesh density corresponded to the "fine mesh" resolution. By eliminating every other mesh point in all three directions, a "coarse mesh" was generated. This coarse mesh resolution was used for both convergence analyses of the fine mesh results, as well as a cost/benefit study. The increased accuracy of the fine mesh (1.26M cells) comes at a significant computational cost, versus the coarse mesh (1.58k cells). All results have been iteratively converged approximately 4 orders of magnitude for the L2 norms. The coarse mesh results exhibit a mass flow consistent to within +-1.0% while the fine mesh exhibits a massflow consistent to within +-0.6%.

The upstream boundary condition for the combustor calculation was created from an axisymmetric inlet calculation that resolved the flowfield from station #1 to station #2 (see Figure 8). The Mach number of the incoming flow was supersonic everywhere except for the nearwall portion of the boundary layer. Thus, the specification of this radial profile as fixed inflow condition to the 3D combustor was a justifiable simplification. Earlier studies of the isolation of downstream pressure disturbances was demonstrated (see DeBonis et al[12]) for this type of geometry. The supersonic outflow boundary condition at station #3 was a simple extrapolation.

The shape of the injector ports was modified so as to simplify the mesh generation process. The experimental rig has gaseous hydrogen lines that supply gaseous H2 to combustor injection ports of a given diameter. The H2 supply is such that a discharge coefficient of 70% has been observed. The computational model has altered the round injector holes by (a) creating an equivalent area square port, and (b) reducing the area to account for the discharge coefficient. The fuel is specified as a sonic, top-hat profile that entered the domain at a mesh boundary that lies flush with the combustor wall. Additionally, a trace amount of atomic Hydrogen (H) was added to the axial jets to ignite the flame-holding region. This amounted to an equivalence ratio for the atomic hydrogen of 0.01, included for all cases presented here. The remaining boundary condition surfaces were specified as either iso-thermal, no-slip walls (1000R) or as symmetry planes.

The three dimensional results of the combustor flowfield are analyzed in the following section. First the dataset is one-dimensionalized in a fashion similar to the stream-thrust-averaging (STA) approach described in Riggins and McClinton[13]. This procedure can yield a great deal of information about the progress of the combustion process. However, care must be taken to properly account for the species mass

flux values in regions of reverse flow. The combustion efficiency (η_c) is stated as the percent of H2 that is present in the form of H2O. In other words, η_c is the portion of fuel that is fully combusted.

RESULTS AND DISCUSSION

ϕ=.6 DATA: COARSE & FINE MESH RESULTS:

Table 1 shows the state of the inlet flow at the entrance of the combustor domain. Keep in mind that the combustor-inflow boundary condition was applied as a radial profile; Table 1 contains a 1D stream-thrust-average of the incoming state for reference purposes only. Table 2 indicates the fuel schedule for this simulation. The results of this calculation appear in the following figures. Figure 9 shows the 1D results and their associated sensitivity to mesh resolution. Note that we can see that there is a measurable difference between the two results for both the 1D Mach number and 1D combustion efficiency. Figure 10 shows a 3D view of the water mole fractions at six cross sections throughout the domain. The coarse and fine mesh results compare quite favorably throughout the constant area section of the combustor. The results begin to diverge throughout the downstream portion of the combustor, differing by 4% at the exit plane. The Mach number profiles look quite similar throughout. Note that as the 1D Mach number approaches unity, a practical limit for upstream fuel injection is approached.

The coarse mesh solution converges in approximately 3000 iterations on four SGI R12000 processors at a wall clock time of about 3.5 days. The fine mesh, (eight times larger) converges after approximately 1500 additional iterations in about two weeks, due to the advantages of mesh sequencing.

The STA data and 3D graphics help to give a feel for the injection strategy employed during this analysis. The presence of H2O clearly indicates the degree to which combustion has occurred. For the ϕ=0.6 case shown in Figure 9 and Figure 10, the burning occurs primarily in the constant area section between the first and second rows of normal injectors. The upstream injectors function quite well and manage to burn the first ϕ=0.4 of fuel in the constant area portion of the combustor. The next ϕ=0.2 of injected fuel seems to take the remainder of the combustor length to burn, but does indeed reach combustion efficiencies in the 90%+ range. However, the flow at the exit of the combustor is rather stratified. A contour plot of oxygen mole fraction (not shown) reveals that a region of oxygen depleted flow sits along the combustor walls on both cowl and centerbody. In order to effectively burn more fuel, we will need to gain access to the oxygen-rich core flow, without approaching the sonic limit for supersonic combustion. The 1D Mach number has dipped to approximately 1.25 with this fuel schedule .

ϕ=.8 DATA: COARSE MESH RESULTS:

The fuel schedule for the ϕ=0.8 condition is given below in Table 3. The difference between ϕ=.6 calculation and ϕ=.8 calculation was that the last row of ports have injected a total of ϕ=0.4, as opposed to ϕ=0.2. Figure 11 is another 3D depiction of the water mole fraction and Figure 12 shows the associated 1D combustion efficiency and Mach number. (Note that the results for the stoichiometric case will be discussed below.) At the exit of the combustor, the combustion efficiency was 88%. For the ϕ=0.6 case, we have completely burned approximately 54% of the available oxygen, while for the ϕ=0.8 case, we have burned approximately 70% of the available oxygen. The minimum 1D Mach number has approached even closer to the sonic limit. It appears from Figure 11 that the increased injector pressure has not only pushed more fuel into the combustor, but improved the jet penetration.

ϕ=1.0 DATA: COARSE MESH RESULTS:

The fuel schedule for the ϕ=1.0 case is given below in Table 4. Note that the only difference from the ϕ=0.6 case was the addition of fuel through the third station of normal injectors. These injectors add an additional ϕ=0.4 of fuel to the combustor flow. This injection occurs in an expansion region and thus the minimal value of Mach number still occurs upstream in the constant area flow. Figure 12 indicates that the combustion efficiency at the exit plane has dropped considerably, as compared to the earlier fuel schedules. The results indicate that we have burned approximately 68% of the available oxygen. Surprisingly, the ϕ=1.0 and the ϕ=0.8 have consumed about the same amount of oxygen. However, for ϕ=1.0, there's a significantly larger lost-thrust-potential due to incomplete combustion.

After considering the results depicted in theFigure 13, the reader notices that the flow has stratified rather than effectively mixed. The expansion region of this annular combustor can be roughly divided into thirds in the radial direction, with an oxygen-rich core, surrounded by fuel rich regions. It appears that for the combustor to effectively burn the remainder of the fuel injected into the expansion region, more mixing must be generated, or the fuel must be injected in such a fashion as to penetrate through the oxygen-depleted regions along both cowl and centerbody walls.

This question of jet penetration has been studied for several decades, and provides a reasonable means of checking one aspect of the CFD. Povinelli and Povinelli[14] have published a correlation for the penetration distance of normal jet injection into a supersonic freestream. The experimental study involved inert gas injection into a constant area flow. However, correlation can be expected to be relevant to the near-field analysis (i.e. first twenty jet diameters, d^*) of our hydrogen injectors in a region of nearly constant area ratio. This is due to the fact that the mixing limited combustion has not consumed much of the fuel stream in the near-field region. The boundary of the fuel jet penetration can be defined as a peak in the thin (OH) layer, along the jet centerline. The mesh resolution of this edge will dictate how accurately we can extract the penetration depth. Consequently, the penetration data has been presented with uncertainty bounds that reflect the local radial cell size. With this definition, we can compare the penetration values predicted with the experimental correlation $(y'/d^*)^{Pov}$ and the values calculated from the CFD results $(y'/d^*)^{CFD}$.

You can see from Figure 14 that the injectors from the ϕ=0.6 and ϕ=0.8 cases have very different penetration values over the first twenty diameters. Despite these differences, the correlation demonstrates that these penetraion values are consistent with the aforementioned experimental data. This is shown in the plot of Figure 15. Notice that the CFD data lie within a +-15% uncertainty bound of the experimental correlation. This (+-15%) bound is representative of the spread in the experimental data from which this correlation is derived. In lieu of a strict validation for this combustor flowpath prediction, the above comparison with experimental data is encouraging. An ability to reliably model the 3D jet injection process will prove to be a significant compliment to our upcoming experimental free-jet data.

SUMMARY AND CONCLUSIONS

We have endeavored to present an overview of the computational combustion research that is currently underway within the GTX program. Detailed computational fluid dynamic simulations for two distinct propulsion modes have been presented. An axisymmetric RBCC engine flowpath was the basis for both sets of CFD analyses.

The numerical simulations of the Independent Ramjet Stream cycle have demonstrated that a flame can be stabilized in the secondary stream, and that the airflow (and therefore the engine pressure) can be adjusted by changing the fuel injection scheme. This ability to control the amount of airflow is essential in order to keep the inlet operating at optimum conditions through the entire Mach number range. The calculations have also allowed us to gain insight into the thermal choke mechanism. In the IRS cycle, the flame propagating across the secondary stream creates an aerodynamic throat that forces the remaining unburned flow to choke.

The scramjet combustor simulations to date have concentrated on Mach 6 freestream flow. The simulations allow for a variety of fuel schedules to be examined quickly in order to optimize the combustor performance. Relatively high combustion efficiencies have been achieved thus far with lean fuel mixtures. The coarse mesh results for combustion efficiency differ by as much as 4% from the fine mesh results. The mesh dependence study indicated that large performance differences (i.e 10% or more) can be analyzed with the coarse mesh density, but relatively fine scale comparisons (i.e. 5% or less) require the more costly fine mesh resolution. Fuel schedule optimization for stoichiometric conditions is currently underway. Both coarse and fine mesh predictions of the normal fuel-jet penetration correlated with similar experimental data to within (+-15%).

Table 1 Inlet flow conditions

variable	*Station #1*	*Station #2*
Ps(psf)	74.12	4816
Ts (R)	390	1454
M	6	2.38
U_{axial} (ft/sec)	5844	4275
U_{radial}	0.	-966

Table 2 Fuel schedule for ϕ=0.6 simulation

Fuel Schedule: ϕ*=0.6 simulation*	*Axial Injector #1*		*Transverse Injector #2*		*Transverse Injector #3*		*Transverse Injector #4*	
	cbdy	*cowl*	*cbdy*	*cowl*	*cbdy*	*cowl*	*cbdy*	*cowl*
Ps (psf)	6739	6739	7964	7964	7964	7964		
Ts (R)	433	433	433	433	433	433		
M	1	1	1	1	1	1		
U_{axial} (ft/sec)	3798	3798	835	---	835	---		
U_{radial}	-835	-835	3798	-3888	3798	-3888		
ϕ^{H_2}	0.1	0.1	0.1	0.1	0.1	0.1		
ϕ^{H}	0.01	0.01	---	---	---	---		

Table 3 Fuel schedule for ϕ=0.8 simulation

Fuel Schedule: ϕ*=0.8 simulation*	*Axial Injector #1*		*Transverse Injector #2*		***Transverse Injector #3***		*Transverse Injector #4*	
	cbdy	*cowl*	*cbdy*	*cowl*	***cbdy***	***cowl***	*cbdy*	*cowl*
Ps (psf)	6739	6739	7964	7964	**18100**	**18100**		
Ts (R)	433	433	433	433	**433**	**433**		
M	1	1	1	1	**1**	**1**		
U_{axial} (ft/sec)	3798	3798	835	---	**835**	**---**		
U_{radial}	-835	-835	3798	-3888	**3798**	**-3888**		
ϕ^{H_2}	0.1	0.1	0.1	0.1	**0.2**	**0.2**		
ϕ^{H}	0.01	0.01	---	---	**---**	**---**		

Table 4 Fuel schedule for ϕ=1.0 simulation

Fuel Schedule: ϕ=*1.0 simulation*	*Axial Injector #1*		*Transverse Injector #2*		*Transverse Injector #3*		***Transverse Injector #4***	
	cbdy	*cowl*	*cbdy*	*cowl*	*cbdy*	*cowl*	***cbdy***	***cowl***
Ps (psf)	6739	6739	7964	7964	7964	7964	**9479**	**9479**
Ts (R)	433	433	433	433	433	433	**433**	**433**
M	1	1	1	1	1	1	**1**	**1**
U_{axial} (ft/sec)	3798	3798	835	---	835	---	**835**	**---**
U_{radial}	-835	-835	3798	-3888	3798	-3888	**3798**	**-3888**
ϕ^{H_2}	0.1	0.1	0.1	0.1	0.1	0.1	**0.2**	**0.2**
ϕ^{H}	0.01	0.01	---	---	---	---	**---**	**---**

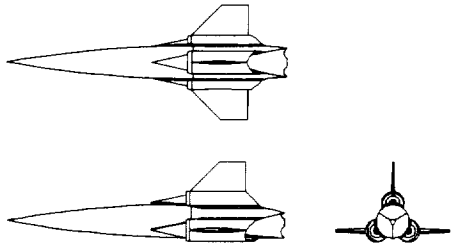

Figure 1. GTX vehicle schematic

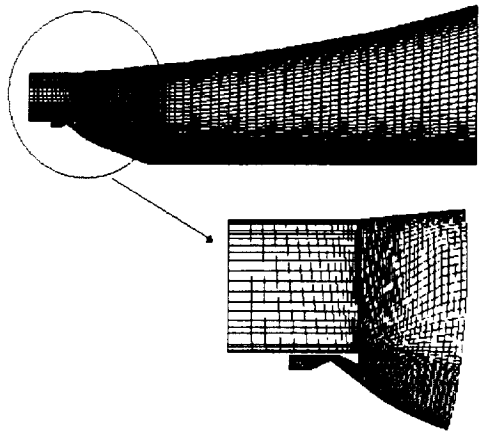

Figure 2. Computational Grid

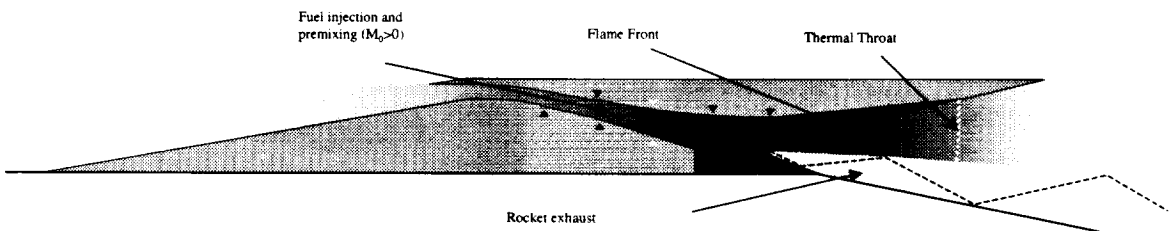

Figure 3. Cross-sectional view of the GTX engine: schematic of the IRS propulsion mode

Flow conditions at M=1 :

Altitude = 10918.7 ft; Free stream pressure = 1408.4 psf; Inlet recovery = 0.95; Rocket chamber pressure = 2000 psi

Secondary stream total pressure = 2532.7 psf ; Secondary stream total temperature = 575.5 R

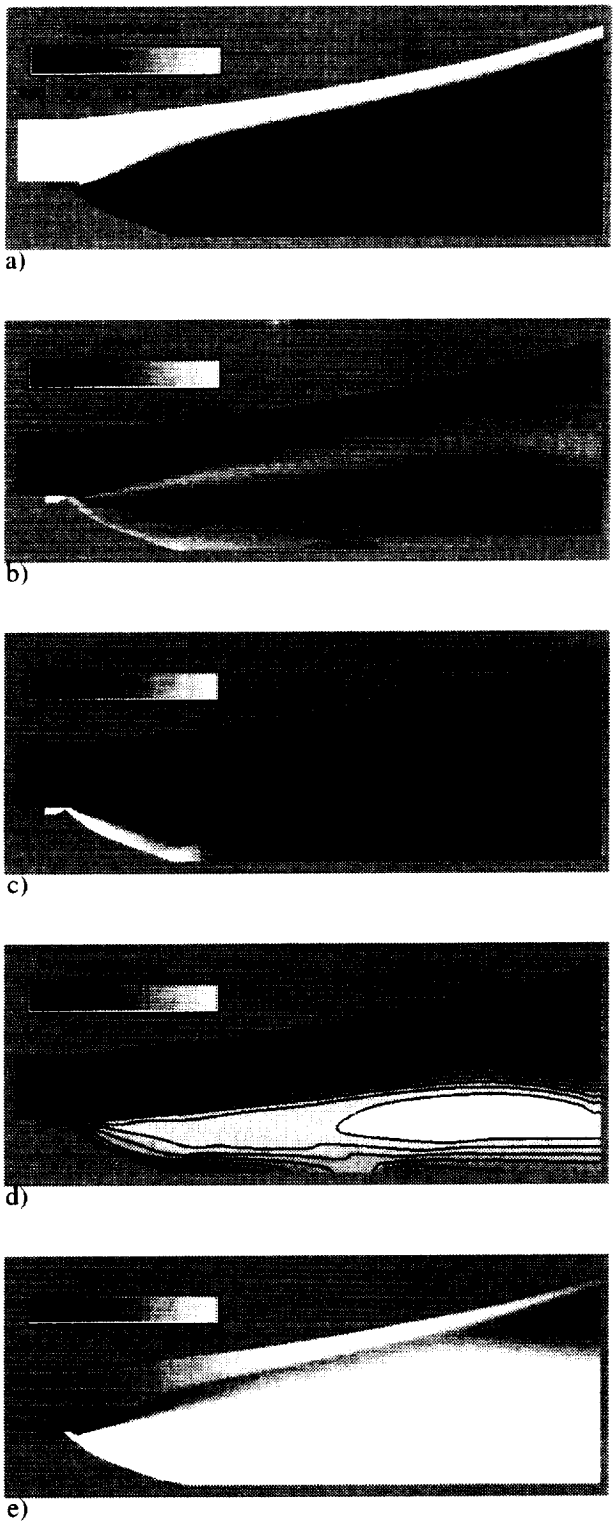

Figure 4. IRS cycle computation at M=1 conditions for a hydrogen-air premixed secondary stream at ϕ=0.6. (Tref=403 R; Pref=3133 psf)

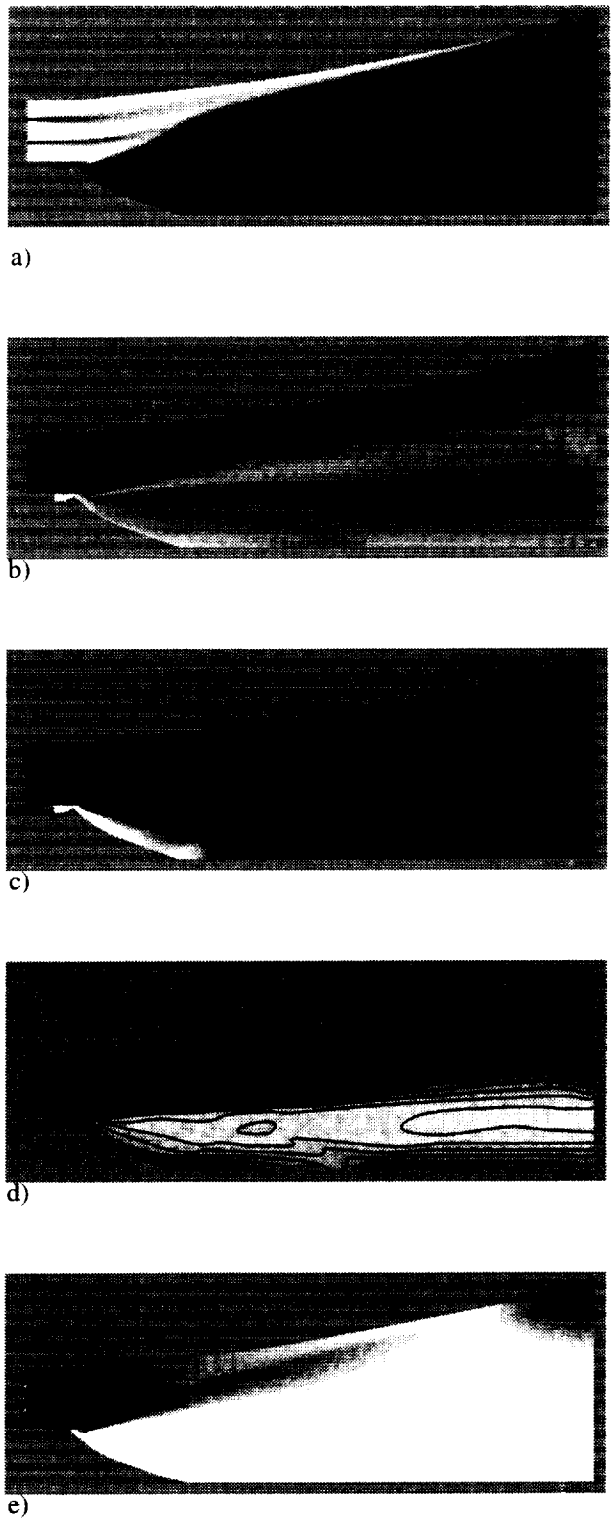

Figure 5. IRS cycle computation at M=1 conditions for two axial hydrogen injectors at ϕ=0.4. (Legends are the same as in Fig. 4)

Flow conditions at M=1.5:

Altitude = 20446.0 ft; Free stream pressure = 957.9 psf; Inlet recovery = 0.925; Rocket chamber pressure = 1393 psi

Secondary stream total pressure = 3252.8 psf ; Secondary stream total temperature = 648.0 R

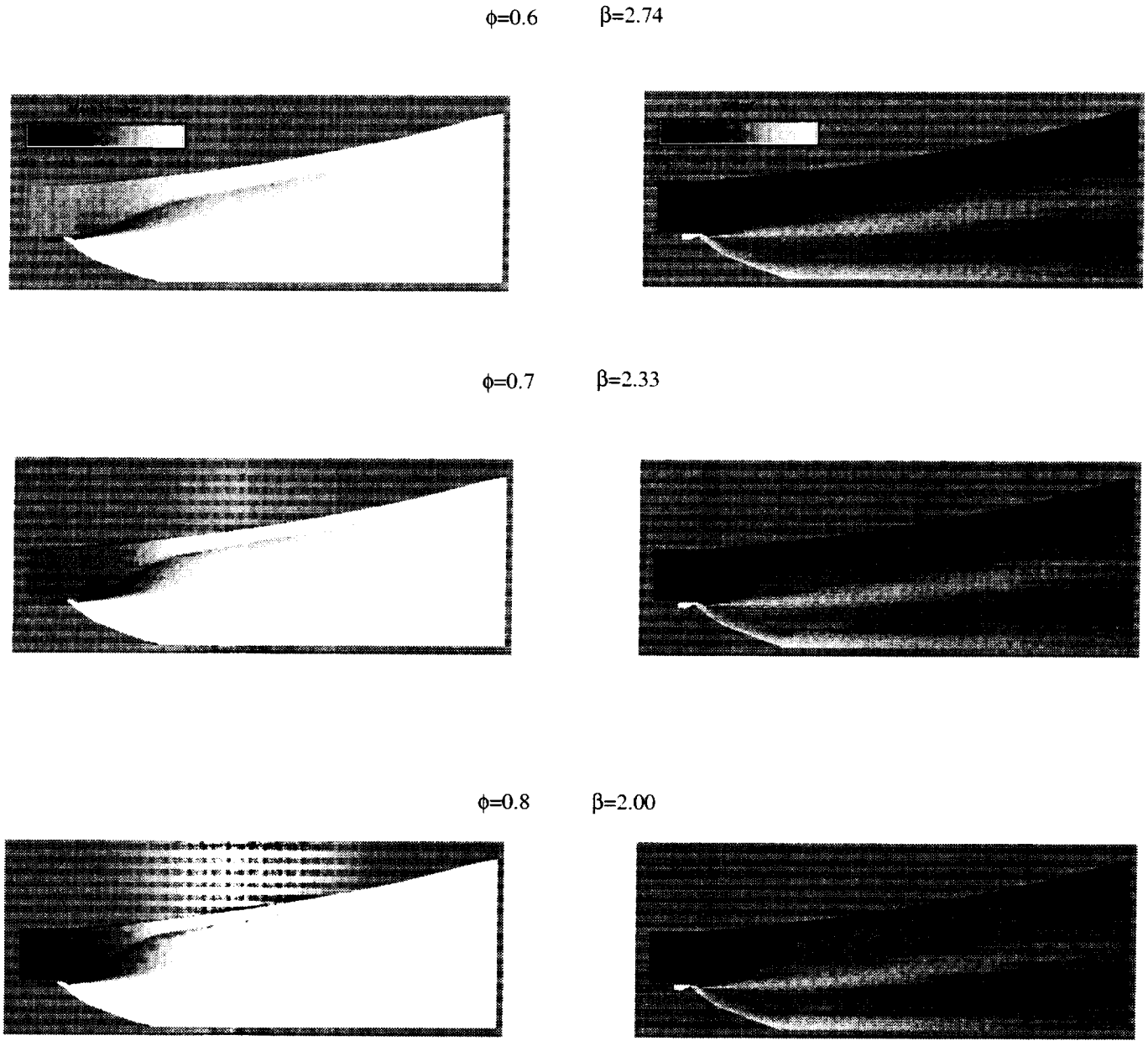

Figure 6. IRS cycle computation at M=1.5 conditions for three different equivalence ratios. (Tref=403 R)

Flow conditions at M=2.0:

Altitude = 33567.0 ft; Free stream pressure = 536.9 psf; Inlet recovery = 0.765; Equivalence ratio = 0.6;

Secondary stream total pressure = 3202.5 psf ; Secondary stream total temperature = 725.0 R

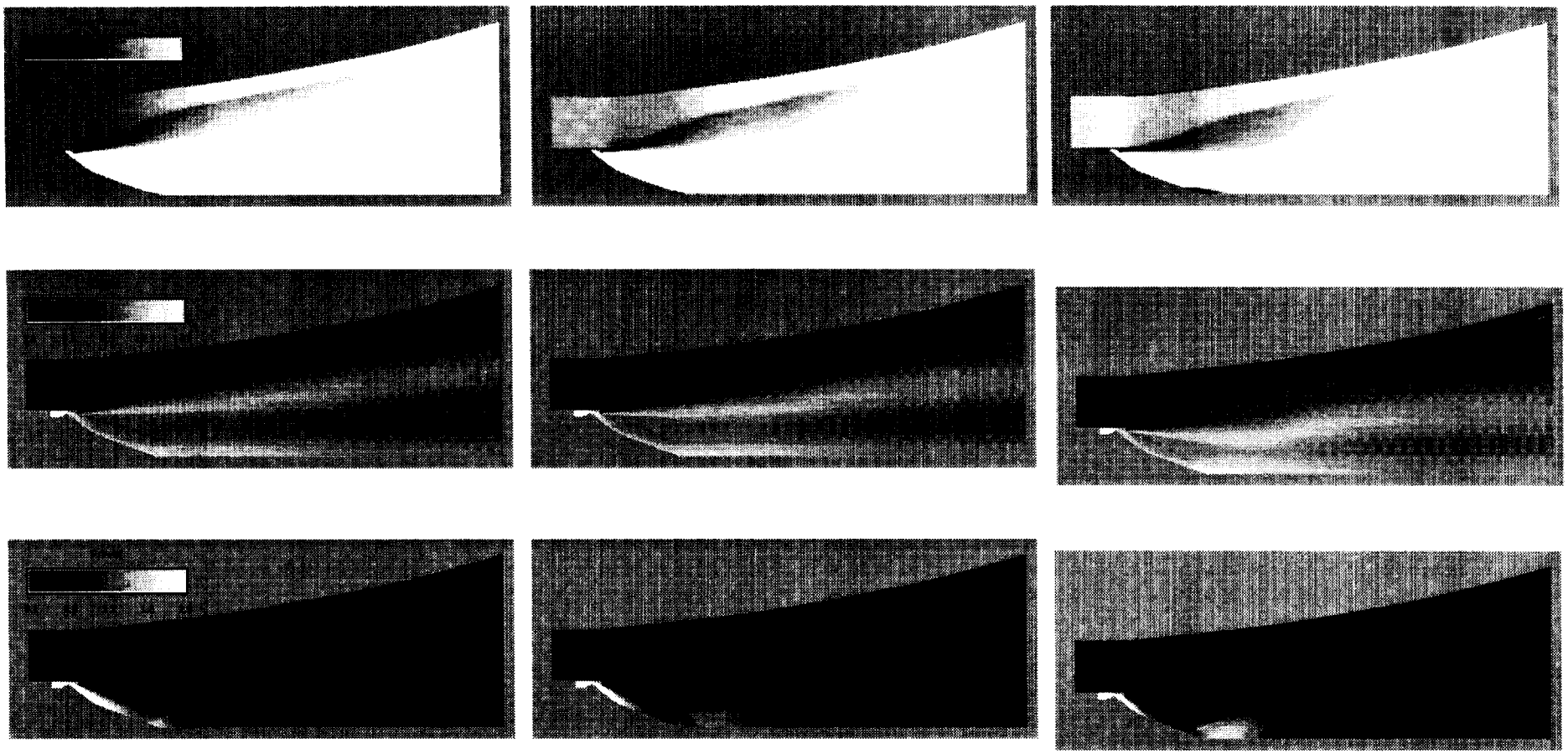

Pc = 1393 psi

Pc = 1000 psi

Pc = 700 psi

Figure 7. IRS cycle computation at M=2.0 conditions for three different rocket chamber pressures (ϕ=0.6). (Tref=403 R; Pref=3133 psf).

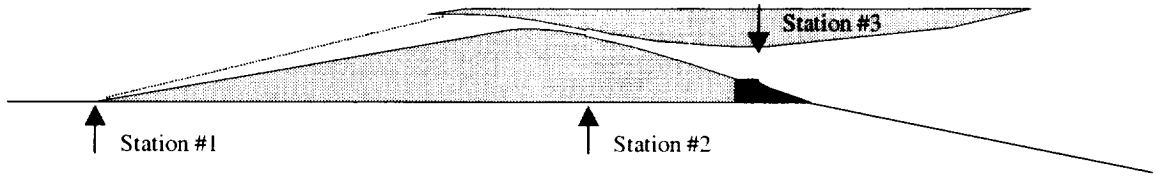

Figure 8 Cross-sectional view of the GTX engine: schematic of the Scramjet propulsion mode

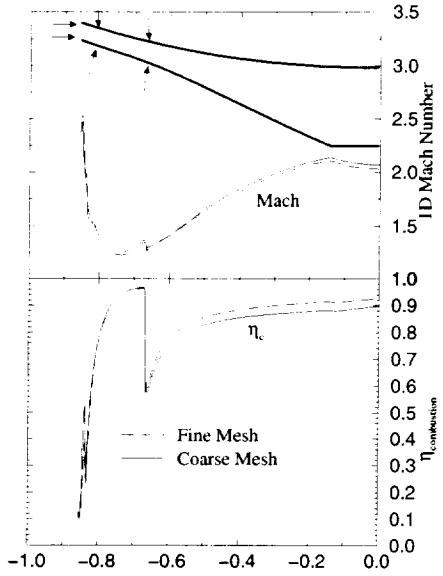

Figure 9 Mesh sensitivity of 1D results: Mach Number and combustion efficiency for ϕ=0.6

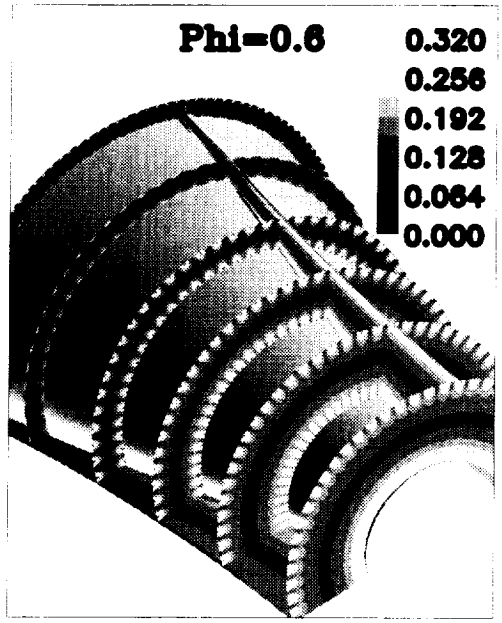

Figure 10 ϕ=0.6 Simulation: H2O mole fraction contour

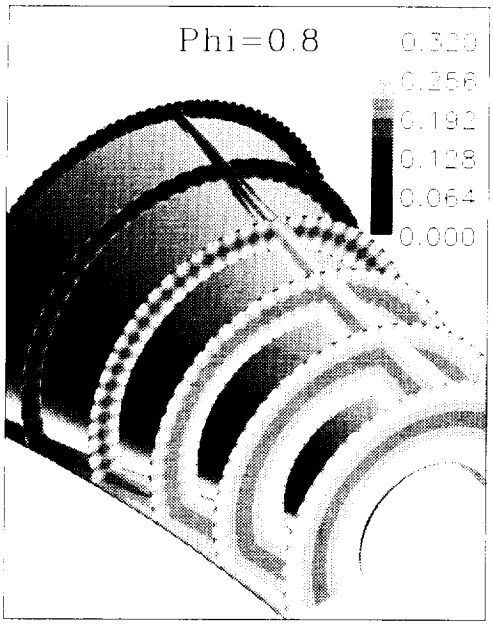

Figure 11 ϕ=0.8 Simulation: H2O mole fraction contours

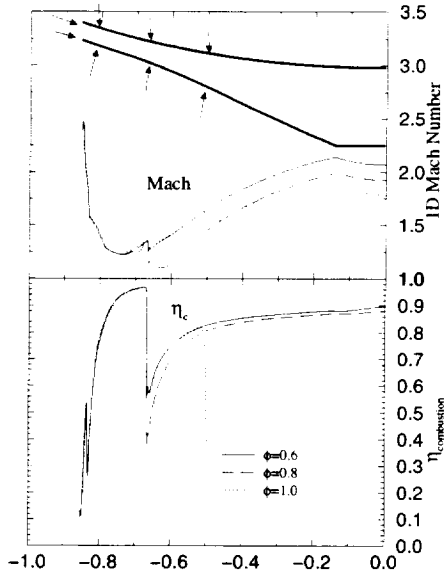

Figure 12 Mach number and combustion efficiency for ϕ=0.6, 0.8 & 1.0

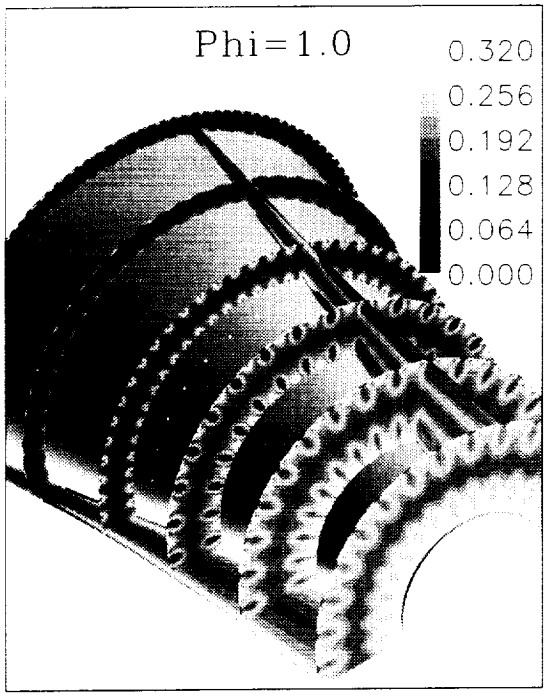

Figure 13 ϕ=1.0 Simulation: H2O mole fraction contours

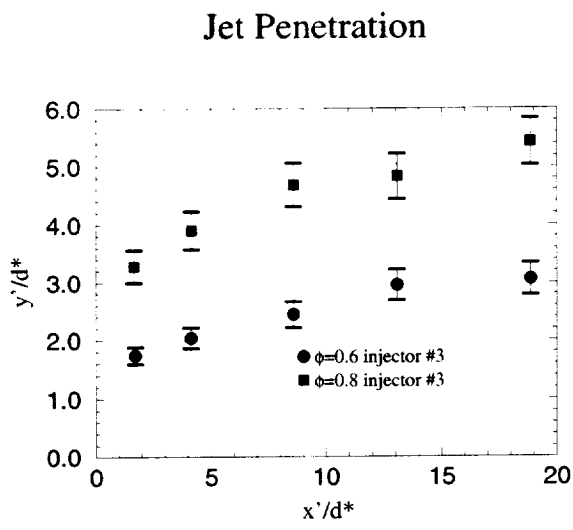

Figure 14 Axial location versus Jet Penetration for CFD data

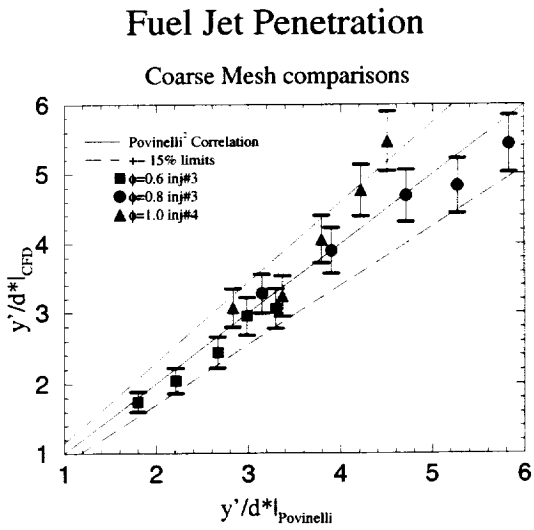

Figure 15 Jet Penetration: experimental correlation versus CFD prediction

REFERENCES

[1] Yungster, S., and Trefny, C. J., "Analysis of a New Rocket-Based Combined-Cycle Engine Concept at Low Speed," AIAA 99-2393, , 35th AIAA/ASME/SAE/ASEE Joint Propulsion Conference and Exhibit, June 20-24, 1999.

[2] Trefny, C. J. "An Airbreathing Launch Vehicle Concept for Single Stage to Orbit," AIAA 99-2730, 35th AIAA/ASME/SAE/ASEE Joint Propulsion Conference and Exhibit, June 20-23, 1999

[3] Yungster, S. and Radhakrishnan, K., "A Fully Implicit Time Accurate Method for Hypersonic Combustion: Application to Shock-Induced Combustion Instability," Shock Waves, Vol. 5, 1996, pp. 293-303.

[4] Spalart, P.R. and Allmaras, S.R., "A One-Equation Turbulence Model for Aerodynamic Flows," La Recherche Aerospatiale, Vol 1, 1994, pp. 5-21.

[5] Jachimowski, C.J., "An Analytical Study of the Hydrogen-Air Reaction Mechanism with Application to Scramjet Combustion," NASA TP-2791, Feb. 1988.

[6] Radhakrishnan, K., "LSENS-A General Chemical Kinetics and Sensitivity Analysis Code for Homogeneous Gas-Phase Reactions. I. Theory and Numerical Solution Procedures," NASA RP-1328, 1994.

[7] Yee, H.C., "Construction of Explicit and Implicit Symmetric TVD Schemes and Their Applications," Journal of Computational Physics, Vol. 68, 1987, pp. 151-179.

[8] GASP Version 3, User's Manual, ISBN 0-9652780-0-X, Aerosoft, Inc., 1996, Blacksburg, VA

[9] Drummond, J. P., Rogers, R. C., and Hussaini, M. Y., "A Detailed Numerical Model of a Supersonic Reacting Mixing Layer," AIAA 86-1427, AIAA/ASME/SAE/ASEE 22nd Joint Propulsion Conference, July, 1986

[10] Gordon, S. and McBride, B. J., "Computer Program for Calculation of Complex Chemical Equilibrium Compositions and Applications; Part I, Analysis," NASA Reference Publication 1311, October 1994, Cleveland, OH

[11] Gridgen Version 13, User Manual, Pointwise, Inc., 1998, Bedford, Texas.

[12] Debonis, J. R., Trefny, C. J. and Steffen, C. J. Jr., "Inlet Development for a Rocket Based Combined Cycle, Single Stage to Orbit Vehicle Using Computational Fluid Dynamics," AIAA 99-2239, 35th AIAA/ASME/SAE/ASEE Joint Propulsion Conference and Exhibit, June 20-24, 1999

[13] Riggins, D. W., and McClinton, C. R., "Analysis of Losses in Supersonic Mixing and Reacting Flows," AIAA 91-2266, 27th AIAA/ASME/SAE/ASEE Joint Propulsion Conference and Exhibit, June 24-26, 1991

[14] Povinelli, F. P., and Povinelli, L. A., "Correlation of secondary sonic and supersonic gaseous jet penetration into supersonic crossflow," NASA TN D-6370, June, 1971.

REPORT DOCUMENTATION PAGE

Form Approved
OMB No. 0704-0188

1. AGENCY USE ONLY (*Leave blank*)	2. REPORT DATE	3. REPORT TYPE AND DATES COVERED
	February 2001	Technical Memorandum

4. TITLE AND SUBTITLE

Computational Analysis of the Combustion Processes in an Axisymmetric, RBCC Flowpath

5. FUNDING NUMBERS

WU–708–65–13–00

6. AUTHOR(S)

Christopher J. Steffen, Jr. and Shaye Yungster

7. PERFORMING ORGANIZATION NAME(S) AND ADDRESS(ES)

National Aeronautics and Space Administration
John H. Glenn Research Center at Lewis Field
Cleveland, Ohio 44135–3191

8. PERFORMING ORGANIZATION REPORT NUMBER

E–12606

9. SPONSORING/MONITORING AGENCY NAME(S) AND ADDRESS(ES)

National Aeronautics and Space Administration
Washington, DC 20546–0001

10. SPONSORING/MONITORING AGENCY REPORT NUMBER

NASA TM—2001-210679

11. SUPPLEMENTARY NOTES

Christopher J. Steffen, Jr., NASA Glenn Research Center, and Shaye Yungster, Institute for Computational Mechanics in Propulsion, Cleveland, Ohio. Prepared for the 37th Combustion Subcommittee, 25th Airbreathing Propulsion Subcommittee, and 19th Propulsion Systems Hazards Subcommittee Joint Meeting cosponsored by the Joint Army-Navy-Air Force Interagency Propulsion Committee, Monterey, California, November 13–17, 2000. Responsible person, Christopher J. Steffen, Jr., organization code 5880, 216–433–8508.

12a. DISTRIBUTION/AVAILABILITY STATEMENT

Unclassified - Unlimited
Subject Categories: 64 and 34 Distribution: Nonstandard

Available electronically at http://gltrs.grc.nasa.gov/GLTRS

This publication is available from the NASA Center for AeroSpace Information, 301–621–0390.

12b. DISTRIBUTION CODE

13. ABSTRACT ***(Maximum 200 words)***

Computational fluid dynamic simulations have been used to study the combustion processes within an axisymmetric, RBCC flowpath. Two distinct operating modes have been analyzed to date, including the independent ramjet stream (IRS) cycle and the supersonic combustion ramjet (scramjet) cycle. The IRS cycle investigation examined the influence of fuel-air ratio, fuel distribution, and rocket chamber pressure upon the combustion physics and thermal choke characteristics. Results indicate that adjustment of the amount and radial distribution of fuel can control the thermal choke point. The secondary massflow rate was very sensitive to the fuel-air ratio and the rocket chamber pressure. The scramjet investigation examined the influence of fuel-air ratio and fuel injection schedule upon combustion performance estimates. An analysis of the mesh-dependence of these calculations was presented. Jet penetration data was extracted from the three-dimensional simulations and compared favorably with experimental correlations of similar flows. Results indicate that combustion efficiency was very sensitive to the fuel schedule.

14. SUBJECT TERMS

Combustion; Propulsion

15. NUMBER OF PAGES

21

16. PRICE CODE

A03

17. SECURITY CLASSIFICATION OF REPORT	18. SECURITY CLASSIFICATION OF THIS PAGE	19. SECURITY CLASSIFICATION OF ABSTRACT	20. LIMITATION OF ABSTRACT
Unclassified	Unclassified	Unclassified	